

Self-consistent prediction of gravitational waves from cosmological phase transitions

Xiao Wang,^{1,*} Chi Tian,^{2,†} and Csaba Balázs^{1,‡}

¹*School of Physics and Astronomy, Monash University, Melbourne, Victoria 3800, Australia*

²*School of Physics and Optoelectronics Engineering,
Anhui University, 111 Jiulong Road, Hefei, Anhui 230601, China*

Gravitational waves from cosmological phase transitions are novel probes of fundamental physics, making their precise calculation essential for revealing various mysteries of the early Universe. In this work we propose a framework that enables the consistent calculation of such gravitational waves sourced by sound waves. Starting from the Lagrangian, this framework integrates the calculation of the dynamics of first-order phase transitions in a self-consistent manner, eliminating various approximations typically introduced by conventional methods. At the heart of our approach is the congruous evaluation of the phase transition hydrodynamics that, at every step, is consistently informed by the Lagrangian. We demonstrate the application of our framework using the SM+ $|H|^6$ model, deriving the corresponding gravitational wave spectrum. Our framework establishes a robust foundation for the precise prediction of gravitational waves from phase transitions.

Introduction— Nearly a decade after the first detection of gravitational waves (GWs) by LIGO and Virgo [1], we are now on the brink of another major milestone: the detection of the stochastic gravitational wave background (SGWB). Preliminary evidence of this may have already been seen from recent Pulsar Timing Array experiments [2–5]. Phase transition gravitational waves (PTGWs), produced by cosmological first-order phase transitions (FOPTs), represent a significant source of SGWB and have been the focus of extensive studies in recent years. In particular, the possibility of an electroweak FOPT is of considerable interest due to its generation of an SGWB peaking around mHz, which is detectable by several proposed space-based experiments, such as LISA [6, 7], TianQin [8], Taiji [9], BBO [10], DECIGO [11], and Ultimate-DECIGO [12]. Furthermore, FOPTs are associated with various extensions of the Standard Model (SM) of particle physics, making PTGWs a novel probe for new physics.

In order to pin down physics beyond the SM, precisely quantifying the associated PTGWs is essential but challenging. During a phase transition, GWs can be produced via three distinct mechanisms: bubble collisions, sound waves and turbulence. Recent studies [13–15] suggest that sound waves are usually the dominant source of PTGWs for thermal FOPTs, for which the scalar+fluid lattice simulations [16–18] are commonly employed to precisely derive the resulting GWs. These simulations require a large simulation volume to accommodate hundreds of bubbles and fine grid spacing to resolve the bubble wall thickness, making them numerically expensive and time-consuming. Additionally, the wall velocity v_w is adjusted by introducing a friction term, a free parameter, into the Higgs equation of motion (EoM).

Meanwhile, the majority of current studies utilise fitting formulae derived from lattice simulations, wherein all hydrodynamic quantities, including the kinetic energy fraction, are estimated by matching the effective potential of a specific particle physics model to a simplified

equation of state (EoS), such as the bag model, through certain phase transition parameters, such as the bubble wall velocity v_w and the strength parameter α , etc. In practice, the bubble wall velocity is left as a free parameter. Depending on v_w , however, the broken power-law fitting formulae tend to deviate from various current analyses [19–25]. These studies suggest that GW spectra generated by sound waves may more closely resemble to double broken-power law and even exhibit more complex features at low frequencies.

To address these challenges, alternative simplified numerical or semi-analytical methods have been proposed, including the hybrid simulation [19, 26], the Higgsless simulation [20], and the sound shell model [21–23, 25, 27–29]. These approaches aim to enhance efficiency while maintaining accuracy. However, all of these methods rely on simplified models of EoS, such as the bag model, and a manually specified wall velocity. These approximations introduce theoretical uncertainties into the GW spectrum.

In this letter, to overcome these drawbacks of various methods, we propose a novel and efficient hydrodynamic-simulation-based framework capable, in principle, of quantifying PTGWs deterministically for any specific particle physics model. As illustrated in the flowchart in Fig. 1, this method starts with the Lagrangian of a given model, from which the effective potential V_{eff} is derived. Utilising this effective potential, the EoS and nucleation rate Γ are directly obtained, enabling the determination of the reference temperature T_* from Γ . With the EoS and reference temperature T_* , the bubble wall velocity v_w and the hydrodynamics prior to bubble collisions can be simultaneously determined by solving the EoM for scalar field and fluid. By generalising the hybrid simulation, our method can then access the hydrodynamics after bubble collisions for more complicated and realistic EoS obtained by the effective potential. Finally, combining the nucleation history, determined by the nucleation rate and wall velocity, with hydrodynamics, the GW spectrum can be

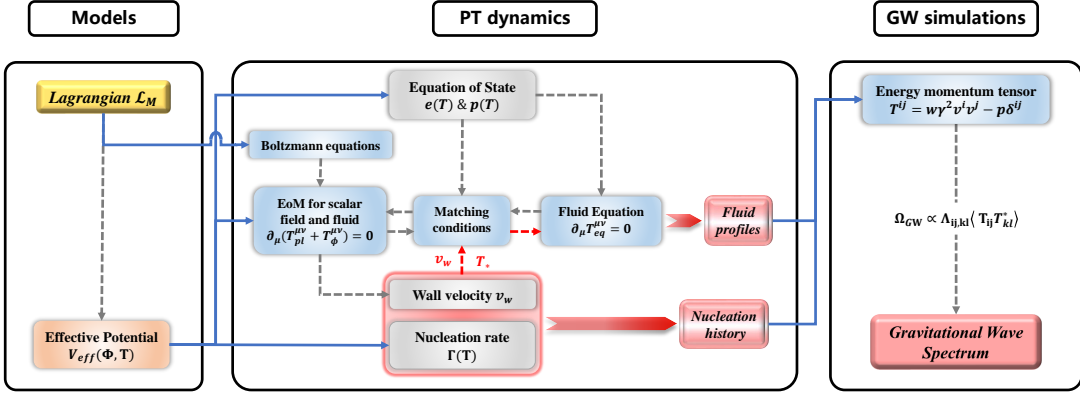


FIG. 1. A schematic flowchart of our calculation framework for phase transition gravitational waves generated by sound waves.

extracted. We validate the applicability of our approach by conducting the first deterministic computation of GW spectra for the SM+ $|H|^6$ model.

Particle Physics Model— We start from the SM+ $|H|^6$ model, which introduces a dimension-6 operator $|H|^6$ to the Lagrangian of the SM [30–34]. The Higgs potential can then be extracted from the effective Lagrangian as

$$V(H) = \mu (H^\dagger H) + \lambda (H^\dagger H)^2 + \frac{1}{\Lambda^2} (H^\dagger H)^3, \quad (1)$$

where the vacuum expectation value of the Higgs Doublet H is $v_{\text{ew}} \equiv \langle H \rangle \approx 246.22$ GeV, Λ denotes the effective cutoff scale, $\lambda = \lambda_{\text{SM}} (1 - \Lambda_{\text{max}}^2/\Lambda^2)$ and $\mu^2 = \mu_{\text{SM}}^2 (-1 + \Lambda_{\text{max}}^2/2\Lambda^2)$. Here, $\Lambda_{\text{max}} = \sqrt{3}v_{\text{ew}}^2/m_h$ with the Higgs mass $m_h \approx 125$ GeV, λ_{SM} and μ_{SM} are the corresponding SM parameters. According to the SM effective field theory, this effective model can represent general characteristics of many new physics models, such as the singlet extension [35–39], two-Higgs Doublet model [40–45], etc. We initiate the study of FOPTs by deriving the effective potential $V_{\text{eff}}(\phi, T)$ of this model. In the unitary gauge, the tree level potential is written as

$$V_{\text{tree}}(\phi) = \frac{1}{2}\mu^2\phi^2 + \frac{1}{4}\lambda\phi^4 + \frac{1}{8\Lambda^2}\phi^6. \quad (2)$$

For simplicity, we approximate the finite-temperature effective potential by adding the thermal mass $cT^2\phi^2/2$ of H to the tree level potential $V_{\text{tree}}(\phi)$, thus

$$V_{\text{eff}}(\phi, T) \approx -\frac{1}{3}aT^4 + \frac{\mu^2 + cT^2}{2}\phi^2 + \frac{\lambda}{4}\phi^4 + \frac{1}{8\Lambda^2}\phi^6, \quad (3)$$

where $a = g_*\pi^2/30$, $g_* \approx 106.75$ is the number of relativistic degrees of freedom at the electroweak phase transition, and $c = \frac{1}{16} \left(g'^2 + 3g^2 + 4y_t^2 + 4\frac{m_h^2}{v_{\text{ew}}^2} - 12\frac{v_{\text{ew}}^2}{\Lambda^2} \right)$. Here g' and g are the $U(1)_Y$ and $SU(2)_L$ gauge couplings, and y_t is the top quark Yukawa coupling. Note that we keep the pure temperature-dependent term $-aT^4/3$ in

the effective potential, as it is necessary for the hydrodynamics of the phase transition.

Phase Transition Dynamics— The dynamics of a thermal first-order phase transition can be, in practice, divided into two parts: the dynamics of the bubble wall, and the hydrodynamics of the plasma. To be able to analyse the dynamics of these two parts, we need to resolve both the EoS and the bubble nucleation rate from the given model. In the thermodynamic limit, the free energy is $\mathcal{F}(T) = V_{\text{eff}}(\phi_m(T), T)$ [46]. Hence, with the effective potential, we can derive the EoS of the SM+ $|H|^6$ as

$$\begin{aligned} p_+(T) &= \frac{1}{3}aT^4, & e_+(T) &= aT^4, \\ p_-(T) &= \frac{1}{3}aT^4 - \frac{\mu^2 + cT^2}{2}\phi_m^2 - \frac{\lambda}{4}\phi_m^4 - \frac{\kappa}{8\Lambda^2}\phi_m^6, \\ e_-(T) &= aT^4 + \frac{\mu^2 - cT^2}{2}\phi_m^2 + \frac{\lambda}{4}\phi_m^4 + \frac{\kappa}{8\Lambda^2}\phi_m^6, \end{aligned} \quad (4)$$

where p_{\pm} and e_{\pm} represent pressure and energy density respectively, subscripts \pm denotes the high-temperature phase and the low-temperature phase, and $\phi_m(T)$ is the global minimum of the effective potential at temperature T . The enthalpy of the system is $w_{\pm} = e_{\pm} + p_{\pm}$.

With the effective potential, one can also derive the nucleation rate $\Gamma(t) = \Gamma_0 \exp[S_E(t)]$, where S_E denotes the bounce action which could be calculated by solving the bounce equation [34]. In this work, to simplify the calculation, we parameterise the bubble nucleation rate as [26, 47]

$$\Gamma(t) \approx \beta_*^4 \exp[\beta_*(t - t_*)], \quad (5)$$

where $\beta_* = \left. \frac{dS_E}{dt} \right|_{t=t_*}$, and the reference time t_* is the time corresponds to the reference temperature T_* . Here, for simplicity, the reference temperature is chosen as the nucleation temperature T_n obtained by the conventional method [34]. In addition to the nucleation rate, understanding the bubble wall velocity [48–53], which characterises the wall dynamics, is crucial for constructing

the full nucleation history. In our framework, the bubble wall velocity is assumed to be a constant and to maintain its steady-state value. Understanding the full nucleation history is also important for hydrodynamics.

Next, we look for ways to determine the steady-state bubble wall velocity v_w . Since v_w is strongly related to the single-bubble hydrodynamics, it must be determined simultaneously while determining the hydrodynamics of a single bubble. The computation begins with the energy-momentum tensor (EMT) of the phase transition system. In general, the EMT consist of the scalar field and the plasma:

$$T^{\mu\nu} = T_\phi^{\mu\nu} + T_{\text{pl}}^{\mu\nu}. \quad (6)$$

Here the EMT of the scalar field is

$$T_\phi^{\mu\nu} = \partial^\mu \phi \partial^\nu \phi - g^{\mu\nu} \left[\frac{1}{2} \partial_\alpha \phi \partial^\alpha \phi - V_0(\phi) \right], \quad (7)$$

with $V_0(\phi)$ being the zero-temperature part of the effective potential, and $T_{\text{pl}}^{\mu\nu}$ representing the EMT of the plasma

$$T_{\text{pl}}^{\mu\nu} = \sum_i \int \frac{d^3 \tilde{\mathbf{p}}}{(2\pi)^3 E_{\tilde{p}}} \tilde{p}^\mu \tilde{p}^\nu f_i. \quad (8)$$

Above, f_i is the distribution function of the particle species i , $\tilde{p}^\mu \equiv (E_{\tilde{p}}, \tilde{\mathbf{p}})$ is the 4-momentum. In both phases, the plasma is in thermal equilibrium and dominates the EMT, thus the scalar field part is negligible. However, across the bubble wall, the contribution of the scalar field should be taken into account, and the plasma becomes out of equilibrium. Assuming the deviation from equilibrium is small, $f_i \approx f_i^{\text{eq}} + \delta f_i$, with $f_i^{\text{eq}} = 1/(\exp[\tilde{p}_\mu u^\mu/T] \pm 1)$, where u^μ is the 4-velocity of the plasma. The EMT of the plasma is then the sum of the equilibrium and the out-of-equilibrium parts, i.e., $T_{\text{pl}}^{\mu\nu} = T_{\text{eq}}^{\mu\nu} + T_{\text{oeq}}^{\mu\nu}$. Here we assume that the plasma is a perfect fluid: $T_{\text{eq}}^{\mu\nu} = (e + p)u^\mu u^\nu - pg^{\mu\nu}$. Based on Lorentz invariance and the symmetry, the out-of-equilibrium EMT can be constructed as $T_{\text{oeq}}^{\mu\nu} = T_{\text{oeq,g}}^{\mu\nu} + T_{\text{oeq,u}}^{\mu\nu}$ [51], with

$$\begin{aligned} T_{\text{oeq,g}} &= \frac{1}{2} \sum_i (m_i^2 \Delta_{00}^i + \Delta_{02}^i - \Delta_{20}^i), \\ T_{\text{oeq,u}} &= \frac{1}{2} \sum_i \left[(3\Delta_{20}^i - \Delta_{02}^i - m_i^2 \Delta_{00}^i) u^\mu u^\nu \right. \\ &\quad \left. + (3\Delta_{02}^i - \Delta_{20}^i + m_i^2 \Delta_{00}^i) \bar{u}^\mu \bar{u}^\nu \right. \\ &\quad \left. + 2\Delta_{11}^i (u^\mu \bar{u}^\nu + \bar{u}^\mu u^\nu) \right]. \end{aligned} \quad (9)$$

The 4-velocity satisfies $\bar{u}^\mu u_\mu = 0$, and

$$\Delta_{mn}^i \equiv \int \frac{d^3 \tilde{\mathbf{p}}}{(2\pi)^3 E_{\tilde{p}}} (\tilde{p}_\mu u^\mu)^m (-\tilde{p}_\mu \bar{u}^\mu)^n \delta f_i. \quad (10)$$

Therefore, in the wall frame, with planar approximation, the total energy-momentum conservation $\partial_\mu T^{\mu\nu}$ at

steady state implies

$$\partial_z^2 \phi + \frac{\partial V_{\text{eff}}}{\partial \phi} + \sum_i \frac{\partial(m_i^2)}{\partial \phi} \frac{\Delta_{00}^i}{2} = 0, \quad (11a)$$

$$\partial_z [w\gamma^2 v + T_{\text{oeq}}^{30}] = 0, \quad (11b)$$

$$\partial_z \left[\frac{1}{2} (\partial_z \phi)^2 - V_{\text{eff}} + w\gamma^2 v^2 + T_{\text{oeq}}^{33} \right] = 0. \quad (11c)$$

Considering the out-of-equilibrium nature of the plasma EMT, eqs. (11) need to be solved simultaneously with the Boltzmann equation to obtain δf_i for every relevant particle species i along with Δ_{mn}^i , which is

$$\left[\tilde{p}_z \partial_z - \frac{1}{2} \partial_z (m_i^2) \partial_{\tilde{p}_z} \right] \delta f_i = \mathcal{C}^{\text{lin}} + \mathcal{S}_i, \quad (12)$$

where the source term \mathcal{S}_i is given by the action of the operator $\hat{\mathcal{D}} \equiv [\tilde{p}_z \partial_z - \partial_z (m_i^2) \partial_{\tilde{p}_z}]/2$ on the equilibrium distribution function f_i^{eq} . The linearised collision terms \mathcal{C}^{lin} can be computed by

$$\begin{aligned} \mathcal{C}^{\text{lin}}[f] &= \sum_a \frac{1}{2N_{\tilde{p}}} \int \frac{d^3 \tilde{\mathbf{k}} d^3 \tilde{\mathbf{p}}' d^3 \tilde{\mathbf{k}}'}{(2\pi)^9 2E_{\tilde{k}} 2E_{\tilde{p}'} 2E_{\tilde{k}'}} |\mathcal{M}_a|^2 (2\pi)^4 \\ &\quad \times \delta^4(\tilde{p} + \tilde{k} - \tilde{p}' - \tilde{k}') \mathcal{P}^{\text{lin}}[f], \end{aligned} \quad (13a)$$

$$\begin{aligned} \mathcal{P}^{\text{lin}}[f] &= f_i^{\text{eq}}(\tilde{p}) f_j^{\text{eq}}(\tilde{k}) f_l^{\text{eq}}(\tilde{p}') f_m^{\text{eq}}(\tilde{k}') \left[\frac{e^{\mathcal{E}_{\tilde{k}}} \delta f_i(\tilde{p})}{f_i^2(\tilde{p})} + \right. \\ &\quad \left. \frac{e^{\mathcal{E}_{\tilde{p}}} \delta f_j(\tilde{k})}{f_j^2(\tilde{k})} - \frac{e^{\mathcal{E}_{\tilde{k}'}} \delta f_l(\tilde{p}')}{f_l^2(\tilde{p}')} - \frac{e^{\mathcal{E}_{\tilde{p}'}} \delta f_m(\tilde{k}')}{f_m^2(\tilde{k}')} \right]. \end{aligned} \quad (13b)$$

Here \tilde{p} denotes the momentum of the incoming particle for which δf is computed, with $N_{\tilde{p}}$ representing its degrees of freedom. The momentum of another incoming particle is \tilde{k} , while \tilde{p}' and \tilde{k}' are the momenta of the outgoing particles. The summation is over all relevant scattering amplitudes $|\mathcal{M}_a|^2$ derived at leading-log order [49–51, 53]. In this work, we only consider the contribution of the top quark to the the friction term in eq.(11a), so the relevant scattering processes include $\bar{t}t \rightarrow gg$, $tg \rightarrow tg$, and $tq \rightarrow tq$. Here g denotes gluons and q represents other quarks, both of which are assumed to be in thermal equilibrium. Additionally, indices i, j, l , and m correspond to different particle species, and $\mathcal{E}_{\tilde{p}} \equiv \tilde{p}_\mu u^\mu$. For simplicity \mathcal{C}^{lin} is calculated in the plasma frame. The Chebyshev spectral method [51, 54] is then employed to solve the Boltzmann equation.

To determine v_w , boundary conditions of eqs. (11) must be applied. These boundary conditions are related to the single-bubble hydrodynamics governed by the EoS (9). Integrating eqs. (11) across the wall gives the matching conditions [55, 56]

$$\begin{aligned} w_+ \gamma_+^2 v_+ &= w_- \gamma_-^2 v_-, \\ w_+ \gamma_+^2 v_+^2 + p_+ &= w_- \gamma_-^2 v_-^2 + p_-. \end{aligned} \quad (14)$$

Our subsequent hydrodynamic analysis shows that the SM+|H|⁶ model allows for detonations ($v_w = |v_+|$), deflagrations ($v_w = |v_-|$), and hybrid modes ($v_- = c_{s,-}$,

	Λ [GeV]	T_n [GeV]	β_n/H_n	v_w	$L_w T_n$
BP ₁	740	95.58	17217	0.43	10.40
BP ₂	640	73.50	1806	0.99995	4.32

TABLE I. The phase transition parameters for two different benchmark points of the SM+ $|H|^6$.

where $c_{s,-}$ is the sound speed just behind the wall). More details on hydrodynamic analysis can be found in our companion paper [57]. While the boundary conditions for the detonation mode can be directly derived from eq. (14), those for the deflagration and hybrid modes require solving the fluid profiles between the bubble wall and the shock front. Since the fluid profiles are away from the bubble wall, it can then be derived from the energy momentum conservation of the plasma in equilibrium, i.e., $\partial_\mu T_{\text{eq}}^{\mu\nu} = 0$ [55, 56]. At steady state, for spherical bubbles, we thus have

$$2\frac{v}{\xi} = \gamma^2(1 - v\xi) \left[\frac{\mu^2}{c_s^2(T)} - 1 \right] \partial_\xi v, \quad (15)$$

$$\partial_\xi T = T\gamma^2 \mu \partial_\xi v.$$

Here, $\mu(\xi, v) \equiv (\xi - v)/(1 - \xi v)$, the sound speed $c_s^2(T) = (dp/dT)/(de/dT)$, $\xi \equiv r/t$, where r denotes the distance from the bubble centre and t is the elapsed times since nucleation. At the shock front, the conservation of the EMT also gives eqs. (14), which determine the position of the shock front. By applying the shooting method, we can thus find corresponding boundary conditions for deflagrations and hybrid modes. We then employ the profile ansatz $\phi(z) = 0.5\phi_0[1 - \tanh(z/L_w)]$, and two moments [49]: $P = -\int dz[\text{Eq.}(11a)]d\phi/dz$, and $G = \int dz[\text{Eq.}(11a)](2\phi/\phi_0 - 1)d\phi/dz$ to simplify the calculation of eqs. (11), where $\phi_0 = \phi_m(T_-)$ and L_w is the bubble wall width. With an iterative method [51], the steady-state bubble wall velocity v_w can be eventually determined and the fluid profiles around a single bubble can also be derived simultaneously from eqs. (15). We show v_w , L_w and other phase transition parameters for two cutoff scales in Table. I. Depending on the cutoff scales, we find that our scheme predicts the existence of a deflagration and a detonation mode for benchmark model BP₁ and BP₂, respectively.

Until now we have derived the important parameters to describe the dynamics before the bubble collision. However, to compute gravitational waves, the hydrodynamics after the collision of bubble walls is essential. To simplify the calculation, we assume the spherical symmetry is still preserved for each radial fluid profile of its corresponding wall surface element, and that the scalar field disappears soon after collisions. The effect of the bubble collision is thus just simply shifting the temperature ahead of the fluid shell to the temperature deep inside the bubbles. Based on energy-momentum conservation $\partial_\mu T_{\text{eq}}^{\mu\nu} = 0$ and

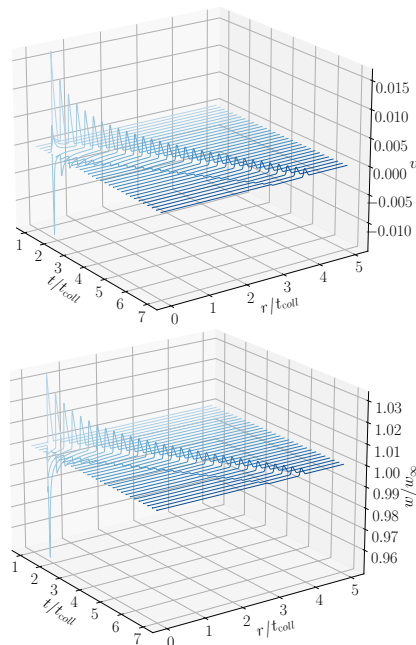


FIG. 2. The evolution of spherically symmetric fluid profiles after collision for benchmark model BP₁. **Top:** the fluid velocity profile. **Bottom:** the enthalpy profile. Here, $w_\infty = w_+(T_n)$ denotes the enthalpy deep inside the high-temperature phase.

the spherical approximation, the equations describing the fluid evolution after collisions are

$$\partial_t E + \partial_r Z = -\frac{2}{r} Z, \quad (16)$$

$$\partial_t Z + \partial_r [Zv + p] = -\frac{2}{r} Zv,$$

where $Z \equiv w\gamma^2 v$ and $E \equiv w\gamma^2 - p$. The Kurganov-Tadmor [58] scheme is used to evolve these equations. We use $E + p - [w + \sqrt{w^2 + 4Z^2}]/2 = 0$ to derive the temperature T with given E and Z . Then with the determined T and the EoS (9), we derive v from the definition of Z with a root finding algorithm. The evolution of fluid profiles of BP₁ are shown in Fig. 2.

So far, we have explored the bubble wall dynamics and hydrodynamics both before and after bubble collisions. Nevertheless, our hydrodynamical analysis only focused on the fluid shell around a single bubble before collision or a single radial fluid element after collision. To access the full hydrodynamics of FOPTs, the hydrodynamics obtained so far should be combined with the full nucleation history. We further assume the system to behave perturbatively, the hydrodynamic quantities could then be given by the superposition of different bubbles:

$$\frac{\Delta w}{w_0}(t, \vec{x}) \simeq \sum_{i:\text{bubbles}} \frac{\Delta w_{\vec{n}_i}}{w_0}(t, |\vec{x} - \vec{n}_i|), \quad (17)$$

$$\vec{v}(t, \vec{x}) \simeq \sum_{i:\text{bubbles}} \vec{v}_{\vec{n}_i}(t, |\vec{x} - \vec{n}_i|).$$

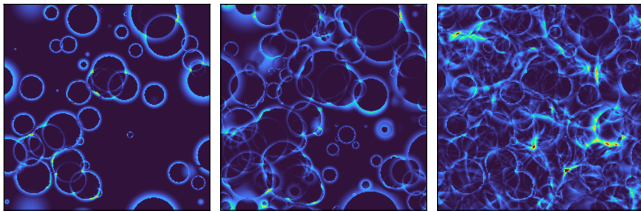


FIG. 3. Snapshots of the time evolution of kinetic energy density $w\gamma^2 v^2(t, \vec{x})$ in our simulations. These figures correspond to a simulation for the benchmark parameter set BP₁ in Table I, with a simulation volume $\mathcal{V} = L^3 = (40v_w/\beta_*)^3$ and grid resolution $N^3 = 256^3$.

Here w_0 is the enthalpy deep inside the bubble, $\Delta w_{\vec{n}_i} = w_{\vec{n}_i} - w_0$, and \vec{n}_i denotes the position vectors of nucleation points. Then, as detailed in Ref. [19, 57], once the collision time of every surface element t_{coll}^i is determined, the 1D spherical solutions can be projected onto a 3D Cartesian lattice as follows. When $t < t_{\text{coll}}$, the radial profile is self-similar and given by eqs. (15), whereas when $t > t_{\text{coll}}$, the radial profile is obtained from eqs. (16). Ultimately, GWs can then be calculated from these 3D quantities given by (17), constructed by 1D profiles.

GW Spectrum— Gravitational waves are characterised by tensor perturbations h_{ij} of the Friedmann-Robertson-Walker metric $ds^2 = -dt^2 + a^2(t)(\delta_{ij} + h_{ij})dx^i dx^j$, sourced by $T^{\mu\nu}$ according to the linearised Einstein equation $\square h_{ij} = 16\pi G\Lambda_{ij,kl}T^{kl}$, where \square and G are the d'Alembertian and the Newtonian constant. Given the short duration of the GW sources, the scale factor $a(t)$ can be neglected. Hence, the GW spectrum Ω_{GW}^* at production time can be derived by

$$\Omega_{\text{GW}}^*(q) \equiv \frac{1}{\rho_{\text{crit}}} \frac{d\rho_{\text{GW}}}{d \ln k} \approx \frac{4H^2 \tau_{\text{sw}}}{3\pi^2 \beta} \frac{q^3 \beta}{w_\infty^2 \mathcal{V} \mathcal{T}} \times \int \frac{d\Omega_{\vec{k}}}{4\pi} \left[\Lambda_{ij,kl} T_{ij}(q, \vec{k}) T_{kl}^*(q, \vec{k}) \right]_{q=|\vec{k}|}. \quad (18)$$

In this equation q is the angular frequency, \vec{k} the momentum of the GW waves, $\Lambda_{ij,kl}$ is the projection on the transverse-traceless part of the energy-momentum tensor T_{ij} , \mathcal{V} the volume of the simulation box, and \mathcal{T} the simulation time. We use $\tau_{\text{sw}} \approx R_*/\sqrt{K_{\text{H}}}$ to estimate the lifetime of the sound waves, where K_{H} is the kinetic energy fraction, which can be derived by the method given in Ref. [59], and the mean bubble separation $R_* = (8\pi)^{1/3} v_w/\beta_*$.

For the sound waves, the transverse-traceless part of the EMT is $T^{ij}(t, \vec{x}) = w(t, \vec{x})\gamma^2(t, \vec{x})v^i(t, \vec{x})v^j(t, \vec{x})$, which can be constructed from the projected enthalpy and velocity fields at different time described in eqs. (17). We demonstrate the 2D slices for the evolution of the kinetic energy density with the previously mentioned projection in Fig. 3. The GW spectrum Ω_{GW}^* at the production time can then be obtained by plugging the

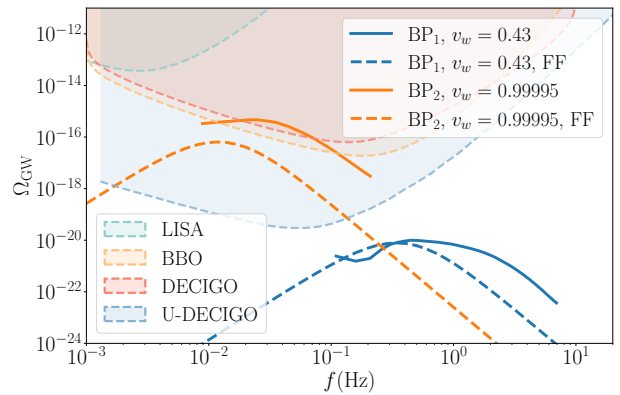


FIG. 4. GW spectra for the benchmark models in Table I. The solid blue line and the solid orange line denote the GW spectra for BP₁ and BP₂, respectively, computed using our scheme. The dashed curves of the same colour represent spectra calculated using fitting formulae. The shaded regions represent the power-law-integrated sensitivity [60, 61] of various ongoing and planned GW detectors.

momentum-space T^{ij} into eq. (18). To obtain the GW spectrum of today, we need to consider the cosmic expansion which yields

$$\Omega_{\text{GW}}(f) = 3.57 \times 10^{-5} \left(\frac{100}{g_*} \right)^{1/3} \Omega_{\text{GW}}^*(q). \quad (19)$$

Above the redshifted frequencies are $f(q) = 2.6 \times 10^{-6} \text{Hz} \frac{q}{\beta} \frac{\beta}{H_*} \frac{T}{100 \text{GeV}} \left(\frac{g_*}{100} \right)^{1/6}$, and H_* is the Hubble parameter obtained by the Friedmann equation at T_* .

In Fig. 4, we show PTGW spectra for the corresponding benchmark models listed in Table I. We find that our scheme predicts that the spectrum of BP₁ falls below the sensitivity of various future GW detectors. In contrast, the spectrum of BP₂ is within the sensitivity range of BBO, DECIGO and Ultimate-DECIGO but remains outside of the sensitivity region of LISA. This can be attributed to the higher phase transition strength. Additionally, we present the result obtained from the fitting formulae of lattice simulations, depicted as dashed curves in Fig. 4. By comparing these spectra, we find that while the peak amplitude of the GW spectrum obtained using our method aligns with the fitting formulae for BP₂, there is a significant discrepancy in amplitude across the accessible frequency range, with the spectral shapes derived from different methods also showing deviations. Additionally, our method suggests the presence of more complex features in the low-frequency range. For BP₂, our approach yields a spectrum with an amplitude approximately an order of magnitude larger and a different shape compared to those predicted by the fitting formulae. Therefore, these comparisons indicate that the conventional fitting formulae may not accurately capture the shape and amplitude of the GW spectrum. Due to the limitations of our current computational resources,

we are unable to compute the spectrum in the low- and high-frequency limit using our method, as these regimes require a larger simulation box and finer grid resolution. Because of this, we only show our GW spectra in a limited frequency range. Outside of this range our present numerical calculation leads to an unphysical rise of the spectrum which indicates the range of its validity.

We also emphasise that although model BP₂ possesses an ultra-relativistic bubble wall velocity, the sound wave remains the dominant source of GWs. This can be demonstrated through the following brief analysis of the energy budget. In general, the energy stored in the wall is $E_{\text{wall}}(t) \approx 4\pi R_b(t)^2 \gamma_w \sigma - \frac{4}{3}\pi R_b(t)^3 \Delta p$ [62, 63], where $\sigma \approx \int dr [\frac{1}{2}(d\phi/dr)^2 + V_{\text{eff}}]$ is the surface tension [46, 64], R_b is the bubble radius, and Δp is the net pressure acting on the wall. Assuming the duration of the initial accelerated expansion is short, $R_b(t) = v_w t$. Further, the net pressure should be zero at steady state, i.e. $\Delta p = 0$. The energy fraction of the wall is defined as $K_{\text{wall}} = E_{\text{wall}}/E_{\text{tot}}$, where $E_{\text{tot}} = \frac{4\pi}{3} R_b(t_*)^3 e_+$. Therefore, at the nucleation temperature, the energy fraction of the wall $K_{\text{wall}} \sim 10^{-10}$. In addition, the kinetic energy fraction of the fluid shell is $K_{\text{fl}} \sim 10^{-4}$. The sound wave is thus still the dominant source of PTGWs.

Conclusion and Outlook— Precise calculations of PTGWs are crucial for accessing new physics beyond the SM with future space-based GW experiments. However, besides theoretical uncertainties induced by the perturbative calculation for the effective potential, the conventional calculations of PTGWs suffer from other inconsistencies such as relying on fitting formulae derived under incompatible assumptions, employing a simplified treatment of the EoS, and leaving the bubble wall velocity as a free parameter. To overcome these inconsistencies, we propose a hydrodynamic-simulation-based framework that allow us to perform the first consistent calculation of PTGWs sourced by the sound waves for the SM+ $|H|^6$. During the calculation of the phase transition hydrodynamics, our framework consistently relies on the Lagrangian instead of using approximations. Compared with the results derived by the conventional method, our results show significant difference both in the spectral shape and amplitude. In summary, our framework represents a significant advancement in the precise calculation of PTGWs. Future improvements could involve incorporating the latest refined calculations of the effective potential [65–68] based on dimensional reduction effective theory [69, 70], which would enable more robust predictions of PTGWs.

Acknowledgments— X.W. would like to thank Benoit Laurent, Henrique Rubira, Michael Bardsley, and Lachlan Morris for enlightening and useful discussions. C.T. is supported by the National Natural Science Foundation of China (Grants No. 12405048) and the Natural Science Foundation of Anhui Province (Grants No. 2308085QA34). X.W. and C.B. are supported

by Australian Research Council grants DP210101636, DP220100643 and LE21010001.

* xiao.wang1@monash.edu

† Corresponding author: ctian@ahu.edu.cn

‡ csaba.balazs@monash.edu

- [1] B. P. Abbott *et al.* (LIGO Scientific, Virgo), “Observation of Gravitational Waves from a Binary Black Hole Merger,” *Phys. Rev. Lett.* **116**, 061102 (2016), [arXiv:1602.03837 \[gr-qc\]](https://arxiv.org/abs/1602.03837).
- [2] Gabriella Agazie *et al.* (NANOGrav), “The NANOGrav 15 yr Data Set: Evidence for a Gravitational-wave Background,” *Astrophys. J. Lett.* **951**, L8 (2023), [arXiv:2306.16213 \[astro-ph.HE\]](https://arxiv.org/abs/2306.16213).
- [3] Heng Xu *et al.*, “Searching for the Nano-Hertz Stochastic Gravitational Wave Background with the Chinese Pulsar Timing Array Data Release I,” *Res. Astron. Astrophys.* **23**, 075024 (2023), [arXiv:2306.16216 \[astro-ph.HE\]](https://arxiv.org/abs/2306.16216).
- [4] J. Antoniadis *et al.* (EPTA, InPTA:), “The second data release from the European Pulsar Timing Array - III. Search for gravitational wave signals,” *Astron. Astrophys.* **678**, A50 (2023), [arXiv:2306.16214 \[astro-ph.HE\]](https://arxiv.org/abs/2306.16214).
- [5] Daniel J. Reardon *et al.*, “Search for an Isotropic Gravitational-wave Background with the Parkes Pulsar Timing Array,” *Astrophys. J. Lett.* **951**, L6 (2023), [arXiv:2306.16215 \[astro-ph.HE\]](https://arxiv.org/abs/2306.16215).
- [6] Pau Amaro-Seoane *et al.* (LISA), “Laser Interferometer Space Antenna,” (2017), [arXiv:1702.00786 \[astro-ph.IM\]](https://arxiv.org/abs/1702.00786).
- [7] Monica Colpi *et al.*, “LISA Definition Study Report,” (2024), [arXiv:2402.07571 \[astro-ph.CO\]](https://arxiv.org/abs/2402.07571).
- [8] Jun Luo *et al.* (TianQin), “TianQin: a space-borne gravitational wave detector,” *Class. Quant. Grav.* **33**, 035010 (2016), [arXiv:1512.02076 \[astro-ph.IM\]](https://arxiv.org/abs/1512.02076).
- [9] Wen-Rui Hu and Yue-Liang Wu, “The Taiji Program in Space for gravitational wave physics and the nature of gravity,” *Natl. Sci. Rev.* **4**, 685–686 (2017).
- [10] Vincent Corbin and Neil J. Cornish, “Detecting the cosmic gravitational wave background with the big bang observer,” *Class. Quant. Grav.* **23**, 2435–2446 (2006), [arXiv:gr-qc/0512039](https://arxiv.org/abs/gr-qc/0512039).
- [11] Seiji Kawamura *et al.*, “The Japanese space gravitational wave antenna: DECIGO,” *Class. Quant. Grav.* **28**, 094011 (2011).
- [12] Hideaki Kudoh, Atsushi Taruya, Takashi Hiramatsu, and Yoshiaki Himemoto, “Detecting a gravitational-wave background with next-generation space interferometers,” *Phys. Rev. D* **73**, 064006 (2006), [arXiv:gr-qc/0511145](https://arxiv.org/abs/gr-qc/0511145).
- [13] Chiara Caprini *et al.*, “Science with the space-based interferometer eLISA. II: Gravitational waves from cosmological phase transitions,” *JCAP* **04**, 001 (2016), [arXiv:1512.06239 \[astro-ph.CO\]](https://arxiv.org/abs/1512.06239).
- [14] Chiara Caprini *et al.*, “Detecting gravitational waves from cosmological phase transitions with LISA: an update,” *JCAP* **03**, 024 (2020), [arXiv:1910.13125 \[astro-ph.CO\]](https://arxiv.org/abs/1910.13125).
- [15] Peter Athron, Csaba Balázs, Andrew Fowlie, Lachlan Morris, and Lei Wu, “Cosmological phase transitions: From perturbative particle physics to gravitational waves,” *Prog. Part. Nucl. Phys.* **135**, 104094 (2024),

- arXiv:2305.02357 [hep-ph].
- [16] Mark Hindmarsh, Stephan J. Huber, Kari Rummukainen, and David J. Weir, “Gravitational waves from the sound of a first order phase transition,” *Phys. Rev. Lett.* **112**, 041301 (2014), arXiv:1304.2433 [hep-ph].
- [17] Mark Hindmarsh, Stephan J. Huber, Kari Rummukainen, and David J. Weir, “Numerical simulations of acoustically generated gravitational waves at a first order phase transition,” *Phys. Rev. D* **92**, 123009 (2015), arXiv:1504.03291 [astro-ph.CO].
- [18] Mark Hindmarsh, Stephan J. Huber, Kari Rummukainen, and David J. Weir, “Shape of the acoustic gravitational wave power spectrum from a first order phase transition,” *Phys. Rev. D* **96**, 103520 (2017), [Erratum: *Phys.Rev.D* 101, 089902 (2020)], arXiv:1704.05871 [astro-ph.CO].
- [19] Ryusuke Jinno, Thomas Konstandin, and Henrique Rubira, “A hybrid simulation of gravitational wave production in first-order phase transitions,” *JCAP* **04**, 014 (2021), arXiv:2010.00971 [astro-ph.CO].
- [20] Ryusuke Jinno, Thomas Konstandin, Henrique Rubira, and Isak Stomberg, “Higgsless simulations of cosmological phase transitions and gravitational waves,” *JCAP* **02**, 011 (2023), arXiv:2209.04369 [astro-ph.CO].
- [21] Mark Hindmarsh, “Sound shell model for acoustic gravitational wave production at a first-order phase transition in the early Universe,” *Phys. Rev. Lett.* **120**, 071301 (2018), arXiv:1608.04735 [astro-ph.CO].
- [22] Mark Hindmarsh and Mulham Hijazi, “Gravitational waves from first order cosmological phase transitions in the Sound Shell Model,” *JCAP* **12**, 062 (2019), arXiv:1909.10040 [astro-ph.CO].
- [23] Alberto Roper Pol, Simona Procacci, and Chiara Caprini, “Characterization of the gravitational wave spectrum from sound waves within the sound shell model,” *Phys. Rev. D* **109**, 063531 (2024), arXiv:2308.12943 [gr-qc].
- [24] Ramkishor Sharma, Jani Dahl, Axel Brandenburg, and Mark Hindmarsh, “Shallow relic gravitational wave spectrum with acoustic peak,” *JCAP* **12**, 042 (2023), arXiv:2308.12916 [gr-qc].
- [25] Lorenzo Giombi, Jani Dahl, and Mark Hindmarsh, “Signatures of the speed of sound on the gravitational wave power spectrum from sound waves,” (2024), arXiv:2409.01426 [gr-qc].
- [26] Ryusuke Jinno, Thomas Konstandin, Henrique Rubira, and Jorinde van de Vis, “Effect of density fluctuations on gravitational wave production in first-order phase transitions,” *JCAP* **12**, 019 (2021), arXiv:2108.11947 [astro-ph.CO].
- [27] Huai-Ke Guo, Kuver Sinha, Daniel Vagie, and Graham White, “Phase Transitions in an Expanding Universe: Stochastic Gravitational Waves in Standard and Non-Standard Histories,” *JCAP* **01**, 001 (2021), arXiv:2007.08537 [hep-ph].
- [28] Xiao Wang, Fa Peng Huang, and Yongping Li, “Sound velocity effects on the phase transition gravitational wave spectrum in the sound shell model,” *Phys. Rev. D* **105**, 103513 (2022), arXiv:2112.14650 [astro-ph.CO].
- [29] Rong-Gen Cai, Shao-Jiang Wang, and Zi-Yan Yuwen, “Hydrodynamic sound shell model,” *Phys. Rev. D* **108**, L021502 (2023), arXiv:2305.00074 [gr-qc].
- [30] Xin-min Zhang, “Operators analysis for Higgs potential and cosmological bound on Higgs mass,” *Phys. Rev. D* **47**, 3065–3067 (1993), arXiv:hep-ph/9301277.
- [31] Christophe Grojean, Geraldine Servant, and James D. Wells, “First-order electroweak phase transition in the standard model with a low cutoff,” *Phys. Rev. D* **71**, 036001 (2005), arXiv:hep-ph/0407019.
- [32] Daniel J. H. Chung, Andrew J. Long, and Lian-Tao Wang, “125 GeV Higgs boson and electroweak phase transition model classes,” *Phys. Rev. D* **87**, 023509 (2013), arXiv:1209.1819 [hep-ph].
- [33] Fa Peng Huang, Youping Wan, Dong-Gang Wang, Yi-Fu Cai, and Xinmin Zhang, “Hearing the echoes of electroweak baryogenesis with gravitational wave detectors,” *Phys. Rev. D* **94**, 041702 (2016), arXiv:1601.01640 [hep-ph].
- [34] Xiao Wang, Fa Peng Huang, and Xinmin Zhang, “Phase transition dynamics and gravitational wave spectra of strong first-order phase transition in supercooled universe,” *JCAP* **05**, 045 (2020), arXiv:2003.08892 [hep-ph].
- [35] Jose Ramon Espinosa and Mariano Quiros, “Novel Effects in Electroweak Breaking from a Hidden Sector,” *Phys. Rev. D* **76**, 076004 (2007), arXiv:hep-ph/0701145.
- [36] Stefano Profumo, Michael J. Ramsey-Musolf, and Gabe Shaughnessy, “Singlet Higgs phenomenology and the electroweak phase transition,” *JHEP* **08**, 010 (2007), arXiv:0705.2425 [hep-ph].
- [37] Jose R. Espinosa, Thomas Konstandin, and Francesco Riva, “Strong Electroweak Phase Transitions in the Standard Model with a Singlet,” *Nucl. Phys. B* **854**, 592–630 (2012), arXiv:1107.5441 [hep-ph].
- [38] Cheng-Wei Chiang, Yen-Ting Li, and Eibun Senaha, “Revisiting electroweak phase transition in the standard model with a real singlet scalar,” *Phys. Lett. B* **789**, 154–159 (2019), arXiv:1808.01098 [hep-ph].
- [39] Peter Athron, Csaba Balazs, Andrew Fowlie, Lachlan Morris, Graham White, and Yang Zhang, “How arbitrary are perturbative calculations of the electroweak phase transition?” *JHEP* **01**, 050 (2023), arXiv:2208.01319 [hep-ph].
- [40] T. D. Lee, “A Theory of Spontaneous T Violation,” *Phys. Rev. D* **8**, 1226–1239 (1973).
- [41] G. C. Branco, P. M. Ferreira, L. Lavoura, M. N. Rebelo, Marc Sher, and Joao P. Silva, “Theory and phenomenology of two-Higgs-doublet models,” *Phys. Rept.* **516**, 1–102 (2012), arXiv:1106.0034 [hep-ph].
- [42] G. C. Dorsch, S. J. Huber, T. Konstandin, and J. M. No, “A Second Higgs Doublet in the Early Universe: Baryogenesis and Gravitational Waves,” *JCAP* **05**, 052 (2017), arXiv:1611.05874 [hep-ph].
- [43] Philipp Basler, Margarete Mühlleitner, and Jonas Wittbrodt, “The CP-Violating 2HDM in Light of a Strong First Order Electroweak Phase Transition and Implications for Higgs Pair Production,” *JHEP* **03**, 061 (2018), arXiv:1711.04097 [hep-ph].
- [44] Duarte Fontes, Margarete Mühlleitner, Jorge C. Romão, Rui Santos, João P. Silva, and Jonas Wittbrodt, “The C2HDM revisited,” *JHEP* **02**, 073 (2018), arXiv:1711.09419 [hep-ph].
- [45] Xiao Wang, Fa Peng Huang, and Xinmin Zhang, “Gravitational wave and collider signals in complex two-Higgs doublet model with dynamical CP-violation at finite temperature,” *Phys. Rev. D* **101**, 015015 (2020), arXiv:1909.02978 [hep-ph].
- [46] Mikko Laine and Aleksu Vuorinen, *Basics of Thermal Field Theory*, Vol. 925 (Springer, 2016) arXiv:1701.01554

- [47] K. Enqvist, J. Ignatius, K. Kajantie, and K. Rummukainen, “Nucleation and bubble growth in a first order cosmological electroweak phase transition,” *Phys. Rev. D* **45**, 3415–3428 (1992). [hep-ph].
- [48] Guy D. Moore and Tomislav Prokopec, “Bubble wall velocity in a first order electroweak phase transition,” *Phys. Rev. Lett.* **75**, 777–780 (1995), arXiv:hep-ph/9503296.
- [49] Guy D. Moore and Tomislav Prokopec, “How fast can the wall move? A Study of the electroweak phase transition dynamics,” *Phys. Rev. D* **52**, 7182–7204 (1995), arXiv:hep-ph/9506475.
- [50] Benoit Laurent and James M. Cline, “Fluid equations for fast-moving electroweak bubble walls,” *Phys. Rev. D* **102**, 063516 (2020), arXiv:2007.10935 [hep-ph].
- [51] Benoit Laurent and James M. Cline, “First principles determination of bubble wall velocity,” *Phys. Rev. D* **106**, 023501 (2022), arXiv:2204.13120 [hep-ph].
- [52] Xiao Wang, Fa Peng Huang, and Xinmin Zhang, “Bubble wall velocity beyond leading-log approximation in electroweak phase transition,” (2020), arXiv:2011.12903 [hep-ph].
- [53] Siyu Jiang, Fa Peng Huang, and Xiao Wang, “Bubble wall velocity during electroweak phase transition in the inert doublet model,” *Phys. Rev. D* **107**, 095005 (2023), arXiv:2211.13142 [hep-ph].
- [54] J.P. Boyd, *Chebyshev and Fourier Spectral Methods: Second Revised Edition*, Dover Books on Mathematics (Dover Publications, 2013).
- [55] Jose R. Espinosa, Thomas Konstandin, Jose M. No, and Geraldine Servant, “Energy Budget of Cosmological First-order Phase Transitions,” *JCAP* **06**, 028 (2010), arXiv:1004.4187 [hep-ph].
- [56] Xiao Wang, Fa Peng Huang, and Xinmin Zhang, “Energy budget and the gravitational wave spectra beyond the bag model,” *Phys. Rev. D* **103**, 103520 (2021), arXiv:2010.13770 [astro-ph.CO].
- [57] Chi Tian, Xiao Wang, and Csaba Balázs, “Gravitational waves from cosmological first-order phase transitions with precise hydrodynamics,” *In preparation*.
- [58] Alexander Kurganov and Eitan Tadmor, “New High-Resolution Central Schemes for Nonlinear Conservation Laws and Convection–Diffusion Equations,” *J. Comput. Phys.* **160**, 241–282 (2000).
- [59] Xiao Wang, Chi Tian, and Fa Peng Huang, “Model-dependent analysis method for energy budget of the cosmological first-order phase transition,” *JCAP* **07**, 006 (2023), arXiv:2301.12328 [hep-ph].
- [60] Eric Thrane and Joseph D. Romano, “Sensitivity curves for searches for gravitational-wave backgrounds,” *Phys. Rev. D* **88**, 124032 (2013), arXiv:1310.5300 [astro-ph.IM].
- [61] Kai Schmitz, “New Sensitivity Curves for Gravitational-Wave Signals from Cosmological Phase Transitions,” *JHEP* **01**, 097 (2021), arXiv:2002.04615 [hep-ph].
- [62] John Ellis, Marek Lewicki, José Miguel No, and Ville Vaskonen, “Gravitational wave energy budget in strongly supercooled phase transitions,” *JCAP* **06**, 024 (2019), arXiv:1903.09642 [hep-ph].
- [63] John Ellis, Marek Lewicki, and Ville Vaskonen, “Updated predictions for gravitational waves produced in a strongly supercooled phase transition,” *JCAP* **11**, 020 (2020), arXiv:2007.15586 [astro-ph.CO].
- [64] Andrei D. Linde, “Decay of the False Vacuum at Finite Temperature,” *Nucl. Phys. B* **216**, 421 (1983), [Erratum: Nucl.Phys.B 223, 544 (1983)].
- [65] Djuna Croon, Oliver Gould, Philipp Schicho, Tuomas V. I. Tenkanen, and Graham White, “Theoretical uncertainties for cosmological first-order phase transitions,” *JHEP* **04**, 055 (2021), arXiv:2009.10080 [hep-ph].
- [66] Philipp Schicho, Tuomas V. I. Tenkanen, and Graham White, “Combining thermal resummation and gauge invariance for electroweak phase transition,” *JHEP* **11**, 047 (2022), arXiv:2203.04284 [hep-ph].
- [67] Oliver Gould and Tuomas V. I. Tenkanen, “Perturbative effective field theory expansions for cosmological phase transitions,” *JHEP* **01**, 048 (2024), arXiv:2309.01672 [hep-ph].
- [68] Andreas Ekstedt, Philipp Schicho, and Tuomas V. I. Tenkanen, “Cosmological phase transitions at three loops: the final verdict on perturbation theory,” (2024), arXiv:2405.18349 [hep-ph].
- [69] K. Farakos, K. Kajantie, K. Rummukainen, and Mikhail E. Shaposhnikov, “3-D physics and the electroweak phase transition: Perturbation theory,” *Nucl. Phys. B* **425**, 67–109 (1994), arXiv:hep-ph/9404201.
- [70] K. Kajantie, M. Laine, K. Rummukainen, and Mikhail E. Shaposhnikov, “Generic rules for high temperature dimensional reduction and their application to the standard model,” *Nucl. Phys. B* **458**, 90–136 (1996), arXiv:hep-ph/9508379.